Eidgenössische Technische Hochschule Zürich
Swiss Federal Institute of Technology Zurich

SED
Schweizerischer Erdbebendienst
Swiss Seismological Service

Report on site characterization

Emmingen, Germany (EMING)

Poggi Valerio, Donat Fäh

Last modified - 24 / 12 / 2014

1. Introduction

In the framework of the NAGRA seismic network project, an array measurement of the ambient vibration wave-field was performed at the location of the SED station EMING (Emmingen, Germany). The scope of the survey is the seismic characterization of the area surrounding the installation (**Figure 1**), which consists in a broadband seismometer (Trillium Compact) with a high-resolution digitizer (Taurus 24Bit @200sps). Ambient vibration analysis has been used to infer the characteristics of the underground structure of the site, with special regard to the one-dimensional shear-wave velocity. Such profile is later used to assess the local seismic response of the station.

For the analysis, different spectral analysis techniques were implemented, consisting in both single and array methods, which are listed below:

- Time-frequency wavelet analysis
- Power-spectral density estimation
- Conventional horizontal to vertical spectral ratios
- Directional horizontal to vertical spectral ratios
- Wavelet polarization analysis
- Three-component high-resolution f-k analysis.

The results of all these analyses conformed to the definition of the final velocity model. In the following, the main results of these investigations are summarized and a final interpretation of the velocity profile is given. From this interpretation, engineering parameters are finally derived, e.g. the Qwl-Vs average velocity, VsZ (including Vs30) and the seismic amplification from the analytical SH-transfer function of the one-dimensional soil column.

2. Survey description

To characterize the seismic response of the site, an array measurement of ambient vibration was performed on 14/08/2014 (**Figure 1**). The array consists of three concentric measuring configurations (called “rings”, R1, R2 and R3) of 11 sensors each and increasing diameter (about 40m, 100m and 200m respectively). The three configurations were planned to partially overlap, with the aim of providing a continuous frequency resolution between the geometries. Configuration R1 recorded for a total of 40m, while configuration R2 for 1h and R3 for 2h30m. The differences in the recording length are due to the different resolution characteristics of the three geometries. As a general rule, larger arrays require longer recording time to produce a reasonable statistics of the ambient vibration processing results. Satisfactory results were obtained from the analysis of the first and last geometry. The second ring did not produce usable results, for reasons later explained. For the larger configuration, a penetration depth of about ~150m was initially expected.

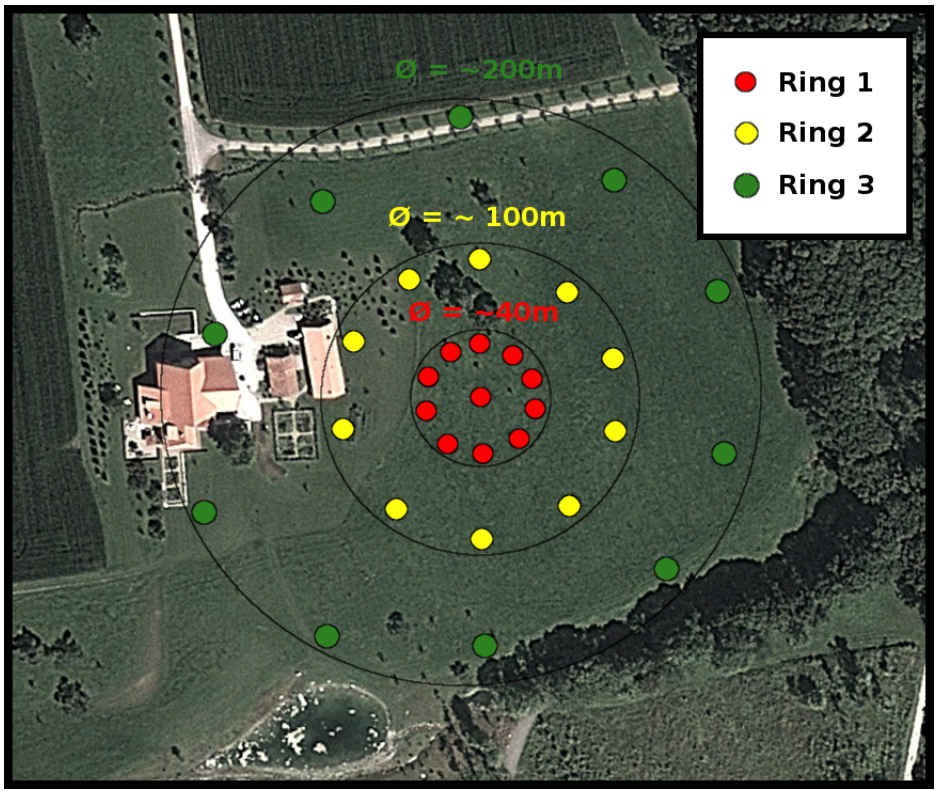

Figure 1 - *Location of the ambient vibration array survey performed in Emmingen (SED station EMING) on 14/08/2014. Three concentric configurations of increasing diameter were implemented (named R1, R2 and R3).*

3. Weather conditions

The weather conditions were good during great part of the measurement, with no precipitations an average temperature of 20 degrees. Some wind was experience during the acquisition of the third ring, as evident from recordings.

4. Soil type, topography and geology

The array has been set in open field conditions, in a rural area (**Figure 1**, **Figure 3**). The influence of buildings and anthropogenic disturbances is virtually negligible. Array sensors have been deployed on free soil. Good coupling with the ground was assured by means of digging small holes at the sensor's places, and by using a special support (*Trihedron*®) that facilitates the leveling of the device even for difficult soil conditions. The measurement area was located on a nearly flat area, and therefore no topographic correction was necessary before processing. The only relevant topographic issue was the presence of a narrow stream valley at the southern edge of the array.

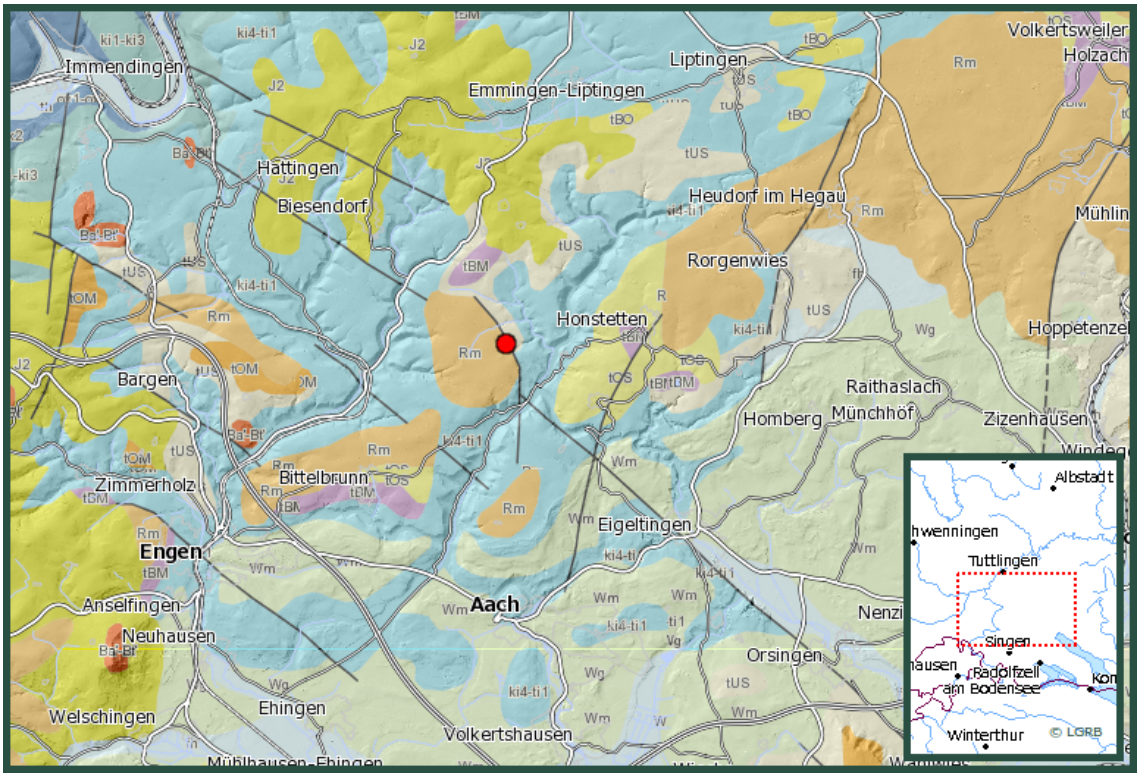

Figure 2 - *Geological map of the measuring area, in the surroundings of Emmingen (reproduced from Geological Atlas LGRB, Baden-Württemberg, modified). In red, the approximate location of the permanent station EMING.*

From the geological points of view (**Figure 2**) the target area sits on bedded limestone and cemented marls of Jurassic age (Kl4-tl1). Geological map shows that calcareous bedrock is in many areas outcropping, but discontinuously covered by spots of Tertiary Molasse sediments (lower Süsswassermolasse, tUS) and Quaternary moraine deposits (Rm). By visual survey, the surface morphology is considerably smooth and modeled by the action of glaciers during the Pleistocene. The station is likely located on top of a morainic deposit. Geophysical bedrock is never exposed at the target site, but likely shallow. A variable-thick cover of quaternary soil material is generally present. Such site can be classified as of rock ground-type A.

5. Acquisition equipment

Each acquisition point within the array consisted of a three components seismometer (Lennartz 3C with 5s eigenperiod) and a 24 bit data logger (Quanterra Q330). Synchronization between stations was assured by standard GPS, while a more accurate differential GPS (Leica Viva system) was used to precisely locate the sensor's coordinates with a tolerance of less than 5cm.

Figure 3 - *Overview of the measurement area taken from the central station of the array (EMN01). SED station EMING is located in background, close to the trees.*

6. Pre-processing and preliminary data-quality control

The three-component recording has been filtered prior to analysis using a band-pass 6th order causal Butterworth filter with corners at 0.2Hz and 50Hz. Although it is not a strict requirement for spectral analysis techniques, such filtering was applied in order to facilitate the preliminary visual inspection of the noise traces and to evaluate the coherency of the wave-field (**Figure 4**). Such procedure gives essential information for the subsequent interpretation of the f-k analysis results.

To assess the quality of the ambient vibration recordings, spectral analysis was subsequently performed. Because of the stochastic nature of the ambient vibration wave-field, a statistical approach has to be used, such as the estimation of the power spectral density (*PSD*). This approach is useful to evaluate the average energy level of the recordings in the analyzed frequency range, and to access the presence of spurious spectral peaks, which might be related to human activity (machinery, pumps). By inspecting the PSD of all the three-component recordings of the array in the range between 0.5 and 40Hz, it is found that the average energy level of the spectrum fits well within the minimum and maximum bounds of the USGS noise model (**Figure 5**), with a progressive increase of energy at high frequency, although no significant peaks of possibly anthropogenic origin are visible.

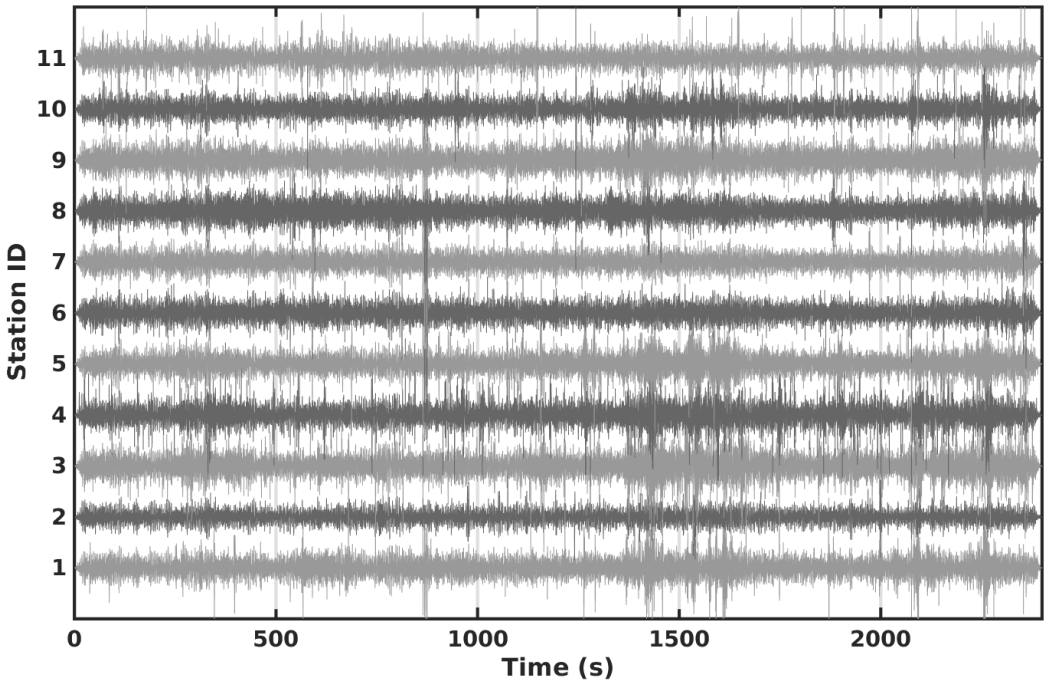

Figure 4 - *Inspection of the useful part of the ambient vibration recording of the Emmingen array (here configuration R1). A certain amount of short high-frequency transients were present during the acquisition, which nevertheless did not bias the subsequent f-k processing results.*

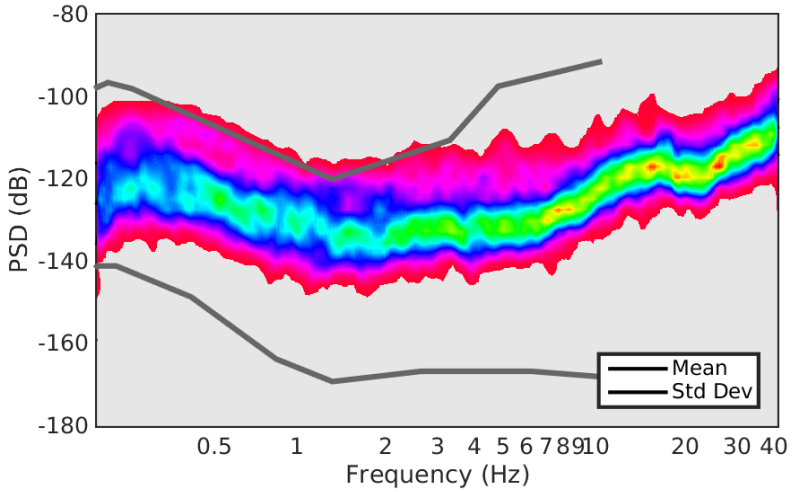

Figure 5 - *Power spectral density (PSD) computed for 40m recording at the central station of the array configuration R1, horizontal direction N-S. Similar results were obtained for the other stations of the array. In gray lines are the minimum and the maximum bounds of the USGS noise model, for comparison.*

Complementary to the aforementioned statistical methods, a spectral decomposition approach is more suitable to assess the stationarity of the ambient vibration wave-field over time. The wavelet time-frequency analysis was then performed over the whole recording time. From such analysis (**Figure 6**) an overall stability of the ambient-vibration wave-field over time is evident. No relevant harmonic signals can be identified in the frequency band useful for the processing, with the exception of a minor contribution at around 20Hz (nevertheless not always present over the whole recordings) and the 50Hz power line effect. These contributions won't likely affect the following processing steps.

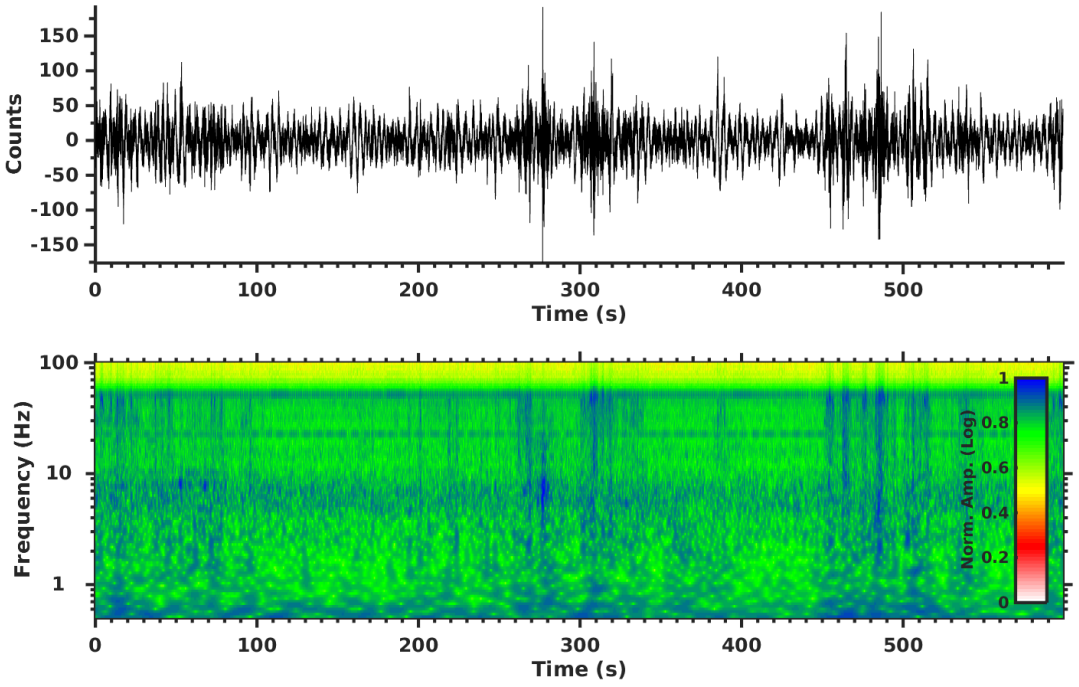

Figure 6 - *Example of spectrogram from 600s of recording of the central station (EMN01) of the array configuration R1, component N-S. No significant harmonic disturbances are visible on the whole spectrogram. Similar results were found for the other components. For the analysis, the cosine wavelet is used (wavelet parameter = 12).*

7. Conventional H/V spectral ratios

The horizontal-to-vertical (H/V) Fourier spectral ratio is a technique widely used in seismic site characterization because of its ability to provide an estimate of the SH wave fundamental frequency of resonance (f_0) of the site. Other than that, H/V ratios are useful to provide information on the Rayleigh wave ellipticity function, which can be used in surface wave dispersion inversion procedures to constrain large velocity contrasts at depth. In this study, we use the H/V technique also to map the variability of the subsoil structure along the investigated area; this is necessary to verify the fulfillment of the 1D structure assumption, which is necessary for the f-k method applied later.

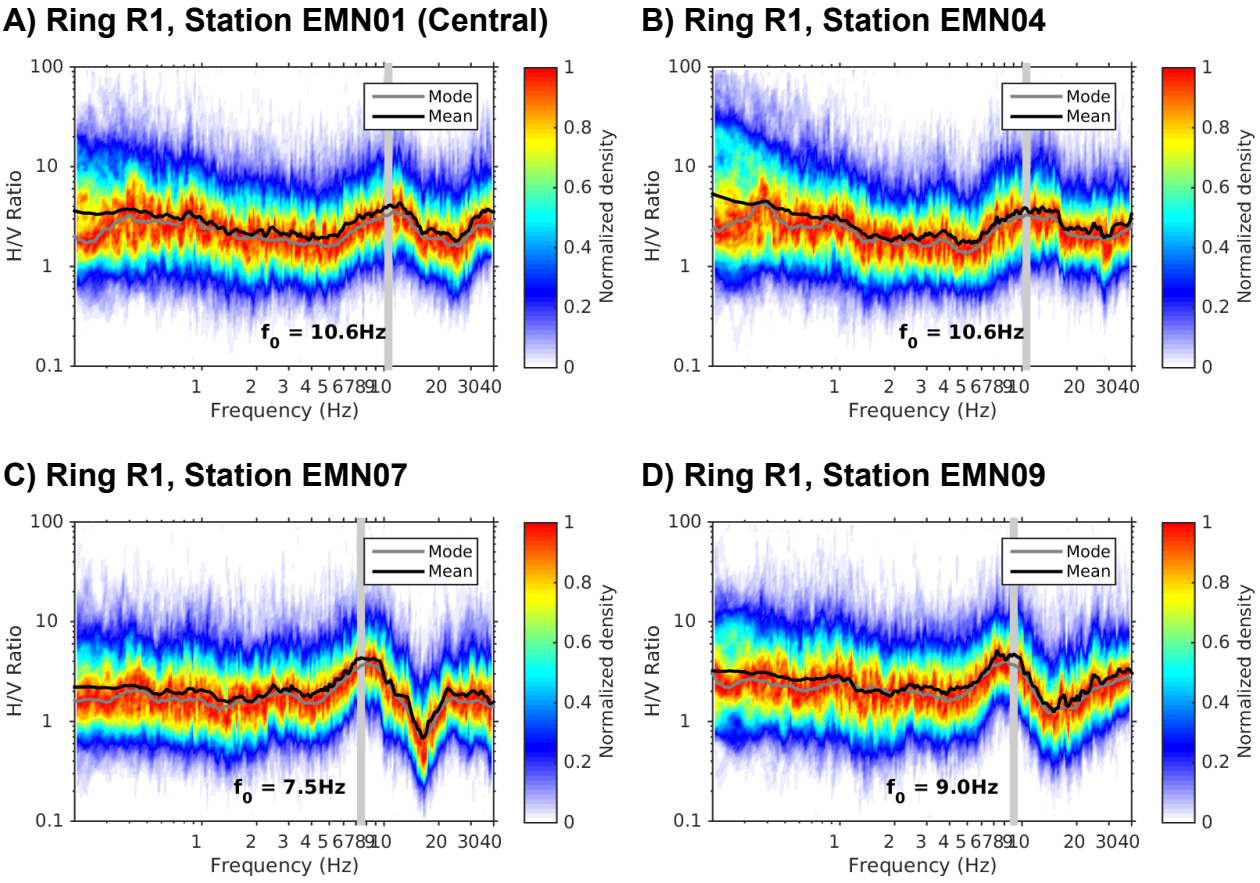

Figure 7 - *Example of H/V spectral ratios for the configurations R1. The resonance frequency of the soil cover is indicated with a light gray line (between about 7 and 11Hz). A very minor peak is visible at about 1Hz (better resolved on the average H/V curve of* **Figure 8***), however of more questionable interpretation.*

H/V spectral ratios have been computed for all the recordings at each station of the array and separately for configurations R1, R2 and R3 (e.g. **Figure 7**). The behavior of the noise wave-field at the different stations location is comparable at low to intermediate frequencies (roughly < 9Hz), while the high frequency region shows some variability, within and between array rings. This is likely due to variability of the top layer, which can be very heterogeneous over the measuring area. Only two stations from the larger configuration (close to the river) exhibited some significant difference with respect to average H/V ratio curves. However, removing these stations from the subsequent processing had no significant impact on the quality of the processing results. Such dissimilarity could then be interpreted as the effect of variability in the local sources, other than heterogeneities in soil conditions.

In average (**Figure 8**), spectral curves show a relatively stable high frequency peak (around 9Hz). Such maximum is likely induced by the presence of shallow bedrock, sheltered by a sediment cover of much lower velocity. An additional peak might be present at very low frequencies (around 1Hz), however of more questionable interpretation. We assume the high frequency peak as the fundamental frequency of the site. The behavior of the site can be considered laterally homogeneous for the f-k analysis.

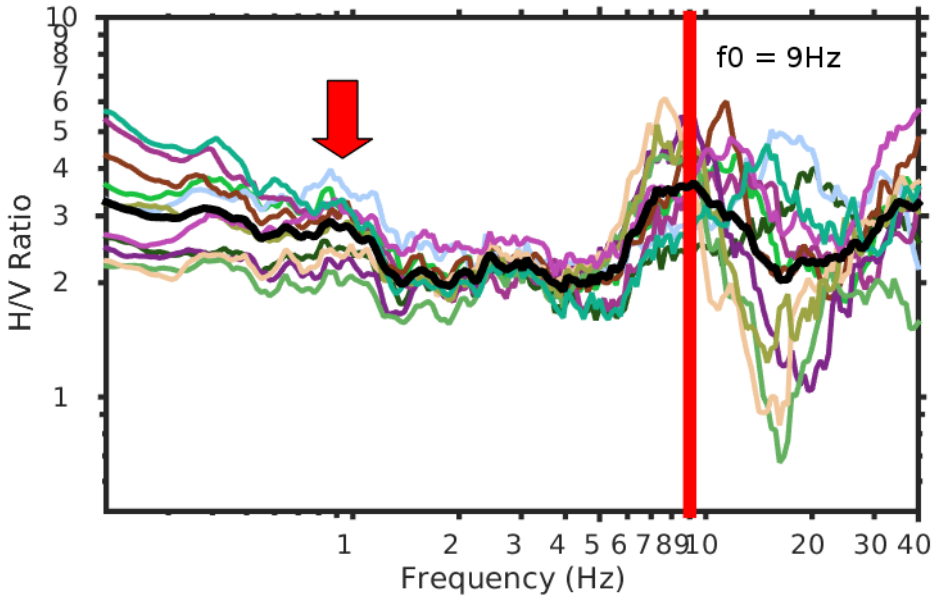

Figure 8 - *Comparison of the H/V spectral ratio curves of all the stations of the array (in this example for the array configuration R1). The curves are generally stable at low frequencies, confirming the lateral homogeneity of the underlying bedrock velocity structure of the site. High frequencies (> 10Hz) show more variability. The average fundamental peak of resonance is at about 9Hz.*

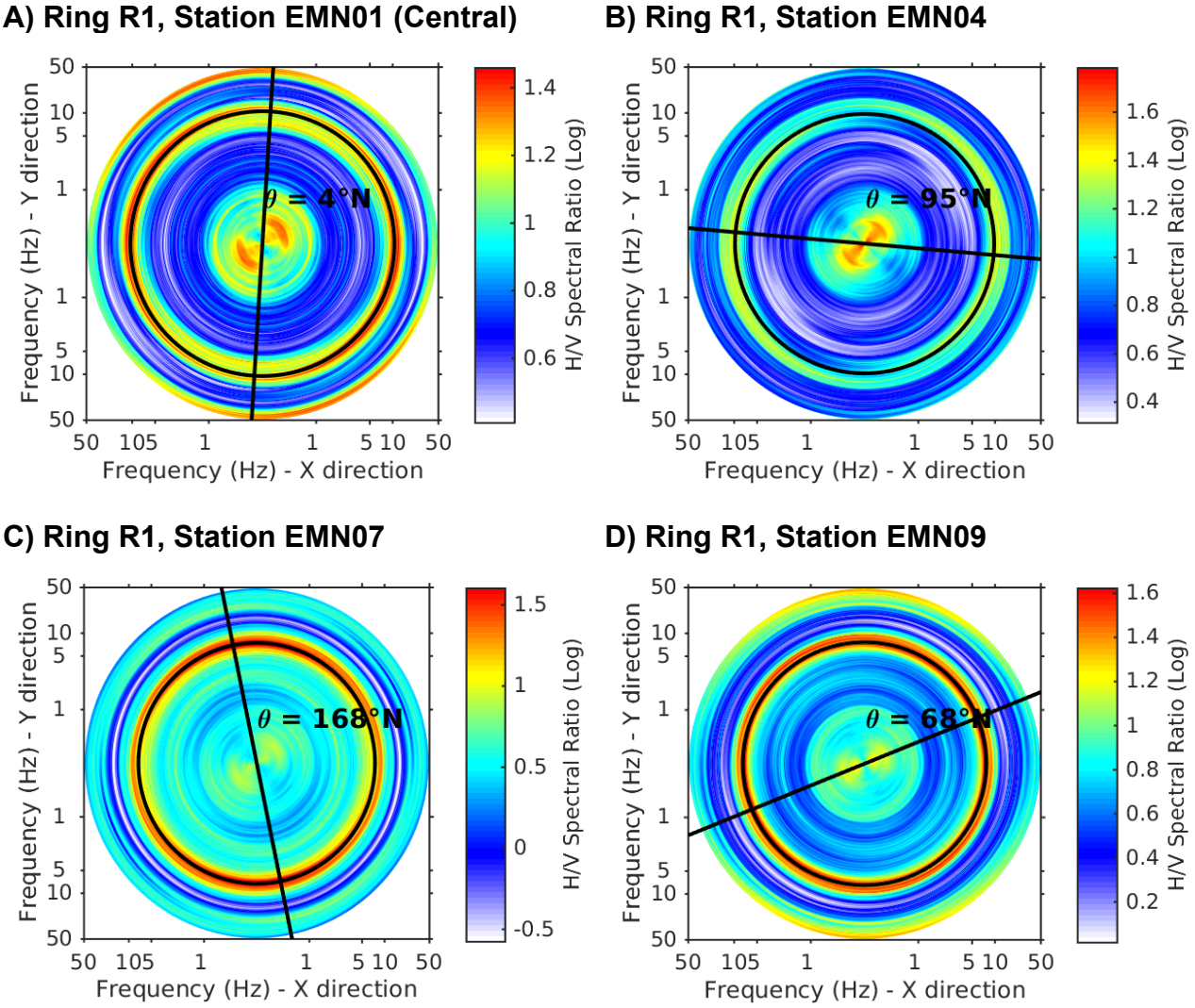

Figure 9 - *Example of directional H/V spectral ratios for configuration R1. No preferential direction of the resonance peak - as well as no evidence of wave-field anisotropy - is present.*

8. Directional analysis

The computation of directional H/V spectral ratio or polarization analysis is useful to reveal asymmetries in the ambient vibration wave-field. Different effects can induce such a behavior: 2D/3D structure, topographic effects or a non-homogeneous distribution of the noise sources. If a strong directionality is found by the analysis, it is generally recommended to carry out further investigations to properly address the origin of polarization. By processing the directional H/V ratios at all the recording stations of the two arrays (e.g. **Figure 9**) it is possible to observe an overall isotropy of the wave-field in the whole analyzed frequency range. In particular, the fundamental frequency peak at about 9 Hz does not show any preferential directionality pattern between the different station locations.

The results of the H/V directional analysis are confirmed by applying the wavelet polarization analysis technique (Burjanek et al., 2008). Here, the particle motion shows to be mostly elliptical, with a significant polarization only at the resonance frequency (**Figure 10**), nevertheless without any sign of azimuthal anisotropy (**Figure 11**A).

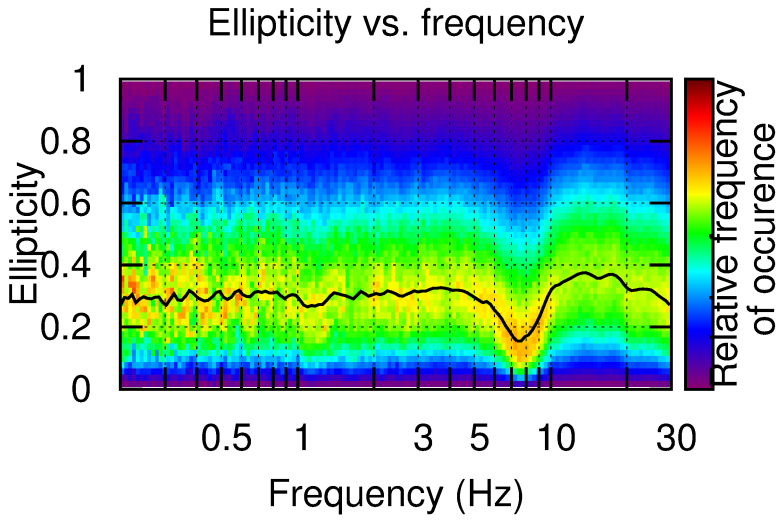

Figure 10 - *Ellipticity of the particle motion from wavelet-based polarization analysis at the central station of the array (EMN01). Similar results can be obtained for other stations of the arrays.*

A)

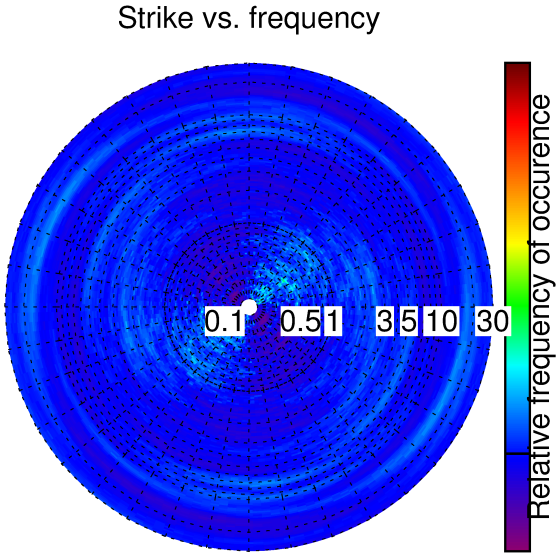

B)

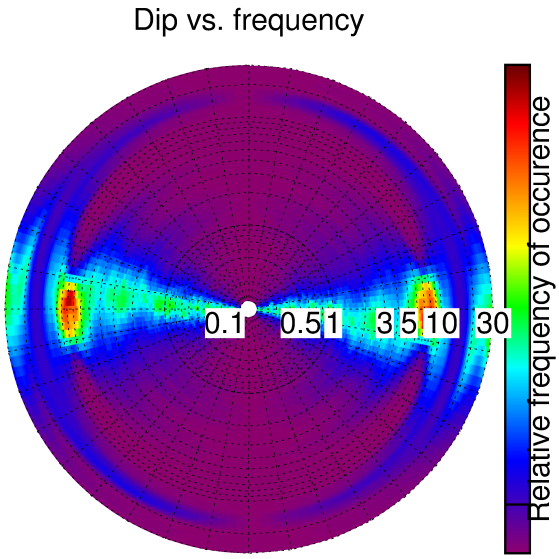

Figure 11 - *Directionality of the particle motion from wavelet-based polarization analysis (dip direction in B, strike in A) at the central station of the array (EMN01). Similar results can be obtained for other stations of the arrays.*

9. Three-component f-k analysis

The frequency-wavenumber analysis is a spectral technique based on seismic array recordings that allows retrieving direction and dispersion characteristics of the surface waves. We apply this technique to three-component ambient vibration recordings using a modification of the high-resolution method of Capon (1969) as described in Poggi et al. (2010). Using all the three-components of motion gives the possibility to retrieve information about the propagation of the Rayleigh waves (vertical and radial processing direction) as well as of the Love waves (transversal direction).

As in the case of the previous methods, the ambient vibration recordings are treated statistically by subdividing the traces in sub-windows. For each consecutive window a separated f-k analysis is performed, and the results are then averaged over the whole recording, increasing the robustness of the final estimation.

A) Ring 3, 5-10Hz

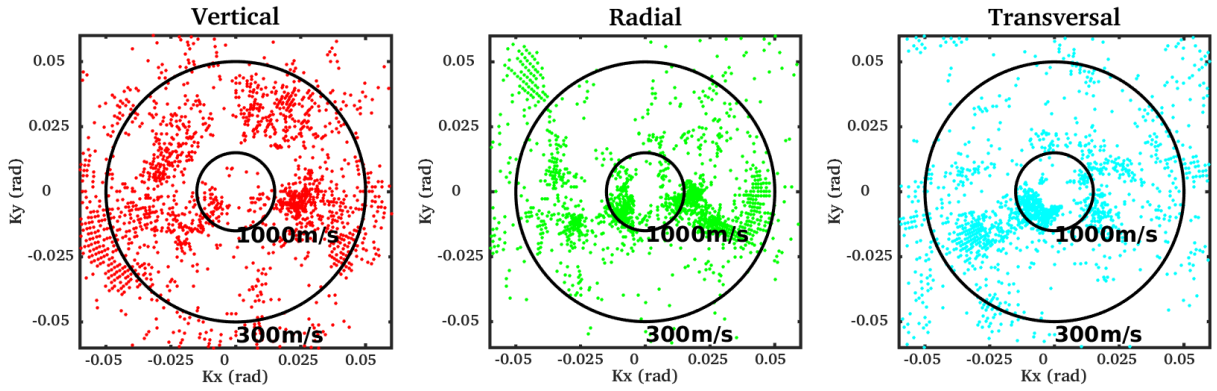

B) Ring1, 10-20Hz

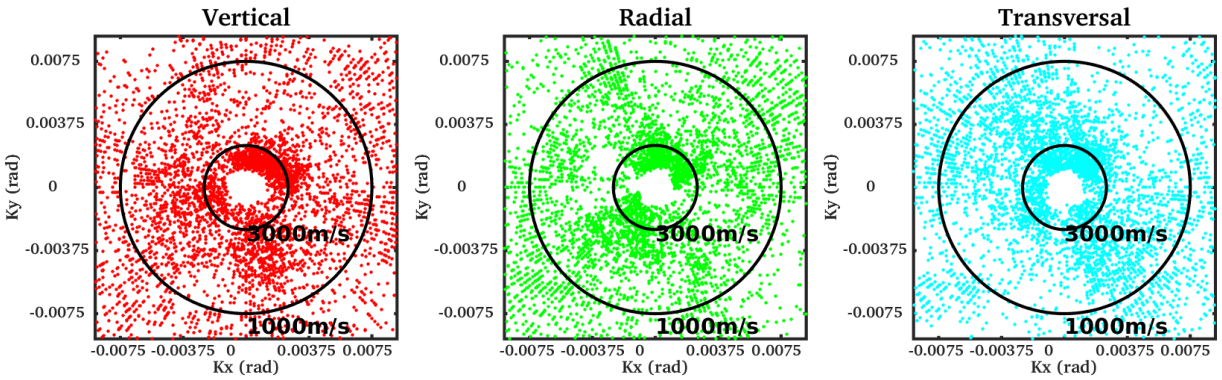

Figure 12 - *Example of distribution of noise sources in the low (5-10Hz) and high frequency range (10-20Hz) obtained from three-component f-k analysis. The source distribution is irregular but not strictly directional on all the propagation components.*

As first step, from the f-k analysis it is possible to assess the azimuthal distribution of noise sources over different frequency ranges (e.g. **Figure 12**) separately for the vertical, the radial and the transversal direction of polarization. From the analysis of the three geometries R1, R2 and R3, source distribution appears to be quite homogeneous in all the components, without displaying a clear directional pattern.

As a second step, the surface-wave dispersion curves are extracted by visual inspection and manual picking of the f-k density plots (**Figure 13** and **Figure 14**), separately for the three polarization directions. Complementary results have been obtained for the array configurations R1 and R3, while R2 did not produce usable results for reasons not yet clarified, but supposedly related to some lack of energy of the surface waves in the intermediate frequency range (as subsequently explained).

In particular, Love wave's fundamental mode dispersion can be well tracked in the frequency range between about 8Hz and 20Hz. Even though the picked dispersion curves present a discontinuity between the two geometries, velocity estimates are quite consistent, which allows extending the mode interpretation from R1 to R3. Same behavior is visible for the Rayleigh wave's fundamental mode, with the additional complication that the high frequency part is visible only on the radial component of R1, while the low frequencies are obtained from the vertical of R3. In a fist attempt we regarded such behavior as a modal jump. However, this hypothesis was later rejected because of incompatibility with the Love component during the inversion process. The running explanation is therefore a simple exchange of energy between vertical and radial directions in the vicinity of the frequency gap (9~10Hz).

A summary of all the identified modes from vertical, radial and transversal direction of propagation is presented in **Figure 15**, while the final interpretation of Rayleigh and Love wave dispersion pattern is in **Figure 16**.

10. Inversion of the dispersion curves

The surface wave dispersion curves (Rayleigh and Love) obtained from the three-component f-k analysis of the ambient vibrations and the fundamental frequency of resonance (f_0) from average H/V spectral ratios are inverted to obtain an estimation of the velocity profile of the site (mainly S-wave velocity as function of depth, and to a lesser extend the P-wave velocity, due to the lower sensitivity). The analysis is performed using the software *Dinver* (www.geopsy.org), which implements a direct search approach (**Figure 17**) based on a conditional version of the neighborhood algorithm (Sambridge, 1999).

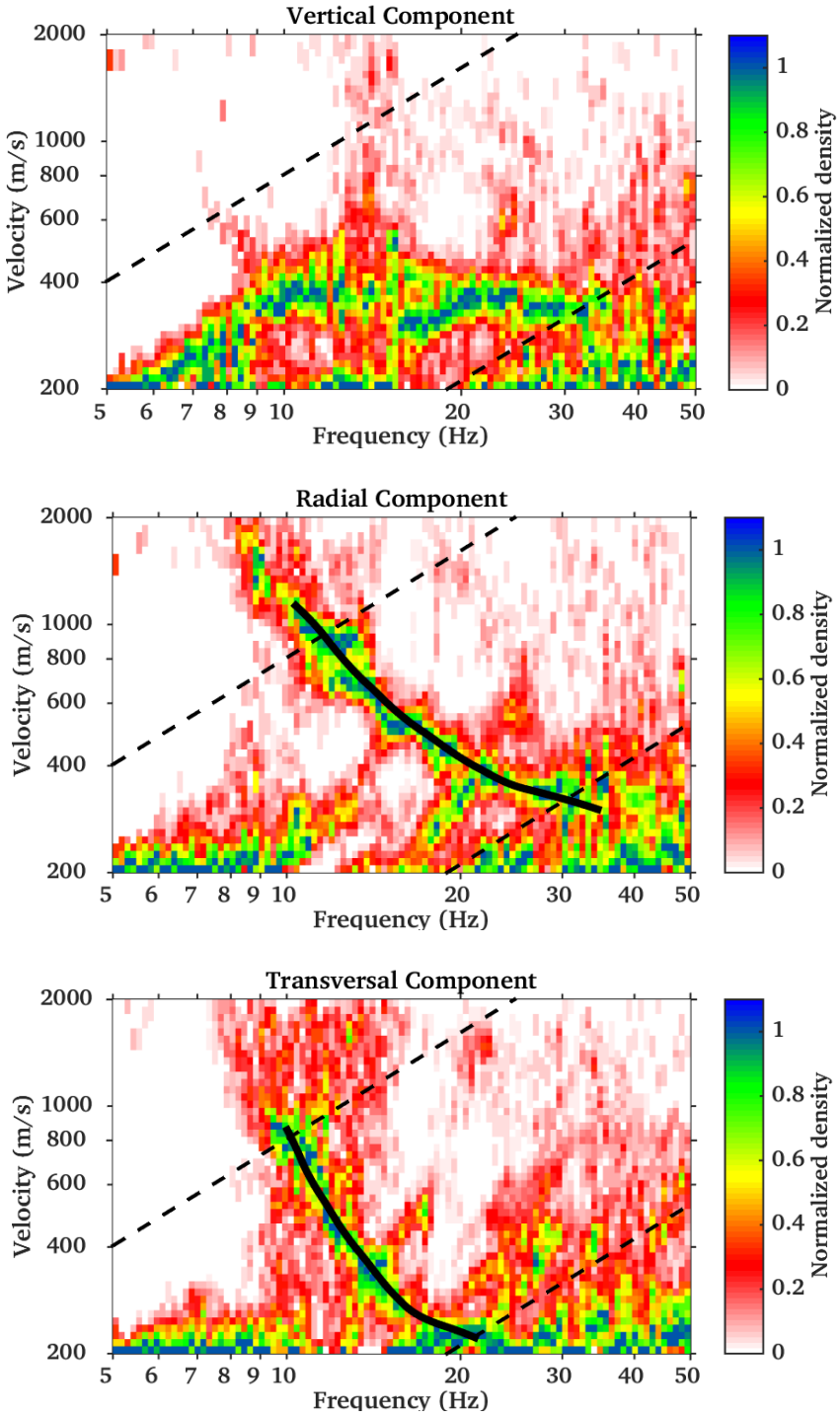

Figure 13 - *Density distribution of the surface wave signals obtained from the recording of the array configuration R1 using three-component f-k analysis. From top to bottom: Rayleigh vertical, Rayleigh radial and Love wave dispersion. In black the interpreted dispersion curves are given (manually selected).*

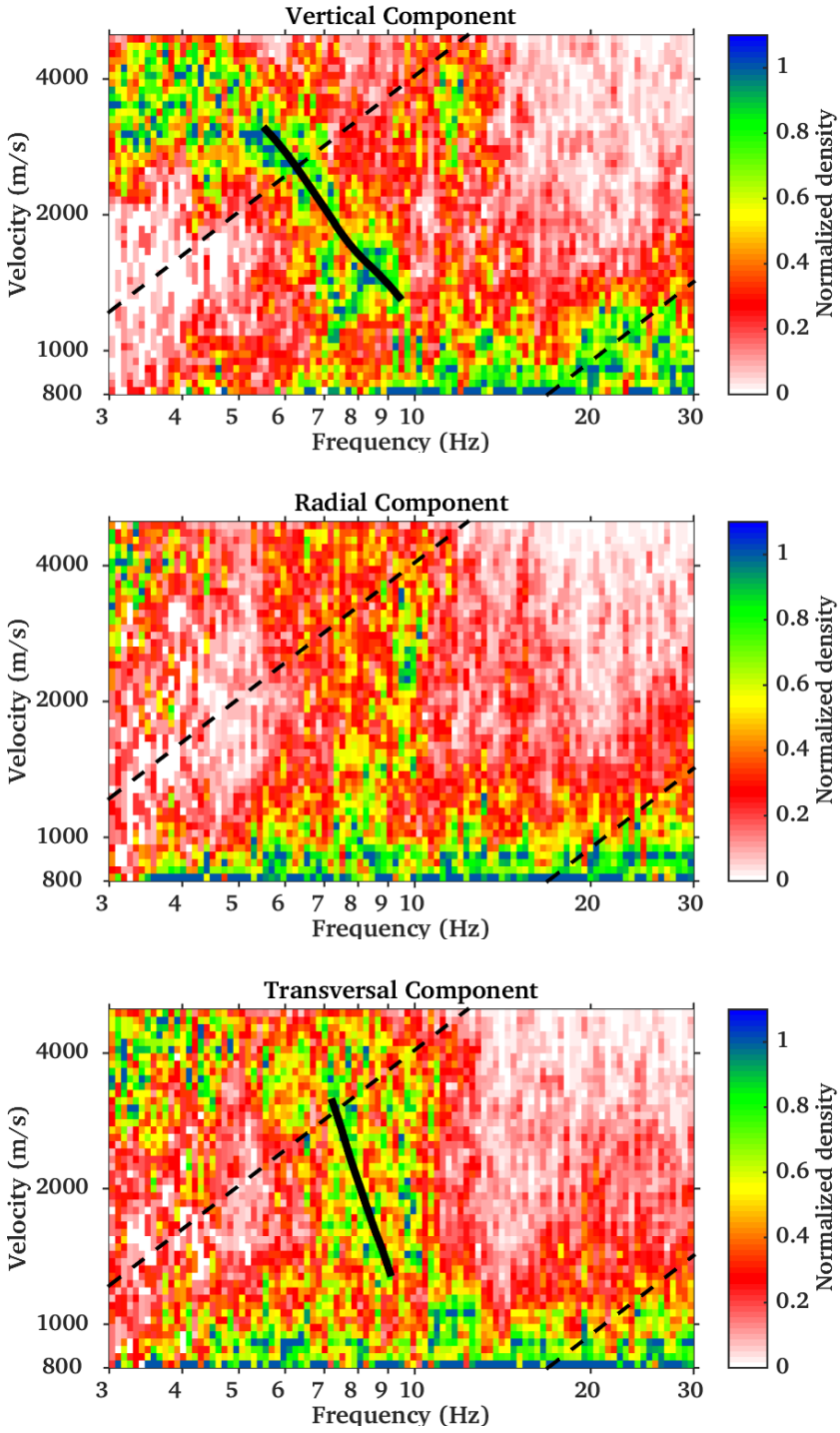

Figure 14 - *Density distribution of the surface wave signals obtained from the recording of the array configuration R3 using three-component f-k analysis. From top to bottom: Rayleigh vertical, Rayleigh radial and Love wave dispersion. In black the interpreted dispersion curves are given (manually selected).*

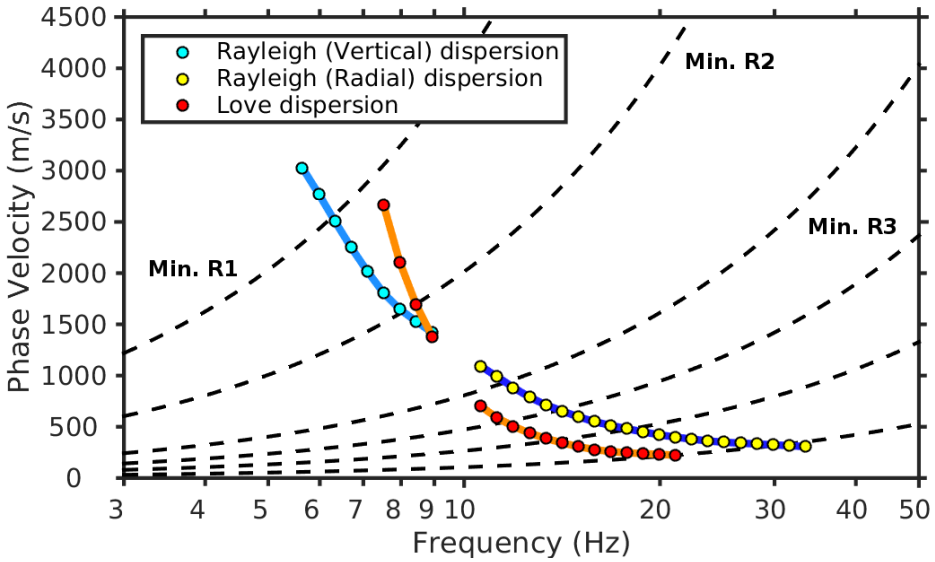

Figure 15 - *Summary of all dispersion curves obtained from three-component f-k analysis of the array configurations R1 and R3. Minimum and maximum resolution bounds from the two geometries are indicated with black dashed lines.*

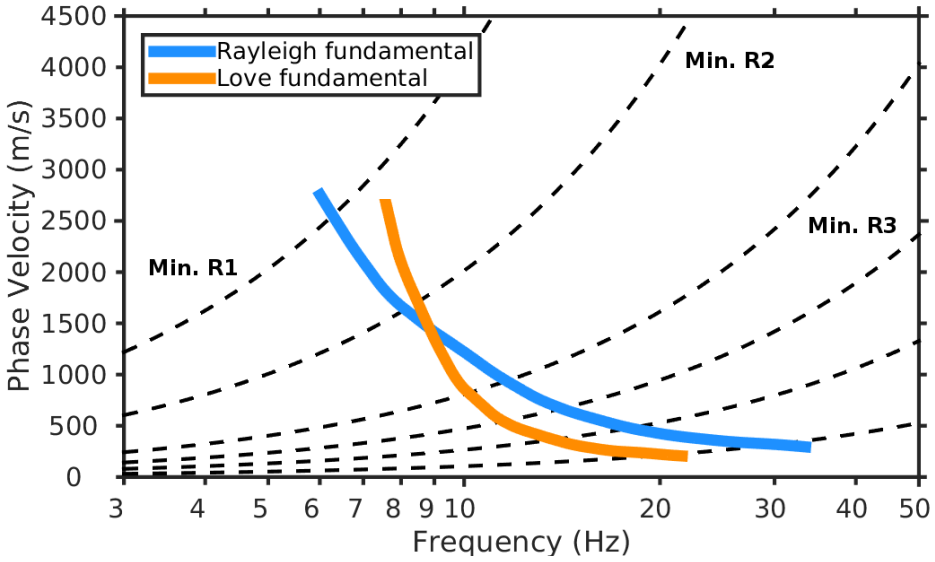

Figure 16 - *Final interpretation of the Rayleigh and Love dispersion curves for EMING. Minimum and maximum resolution bounds from the full array are indicated with black dashed lines.*

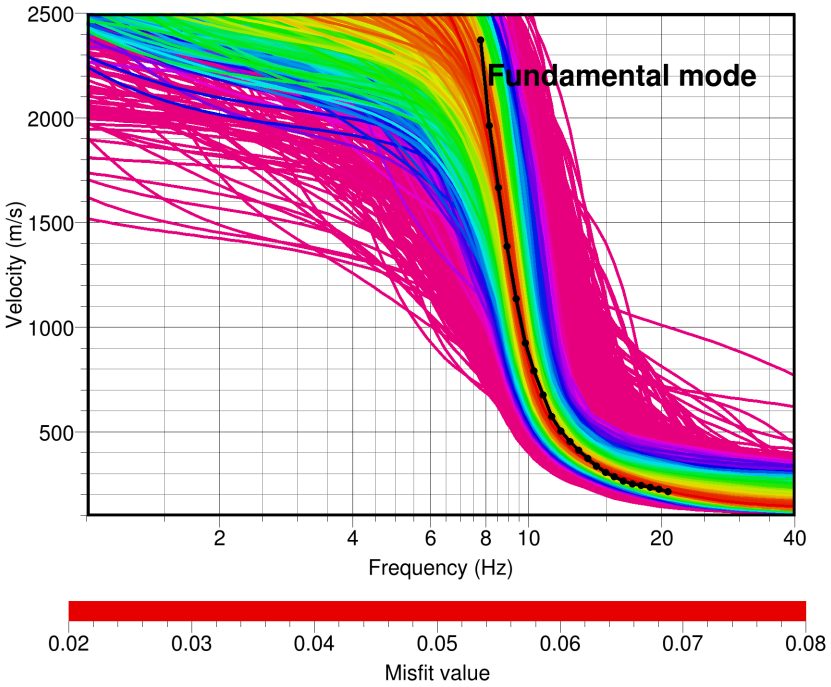

A)

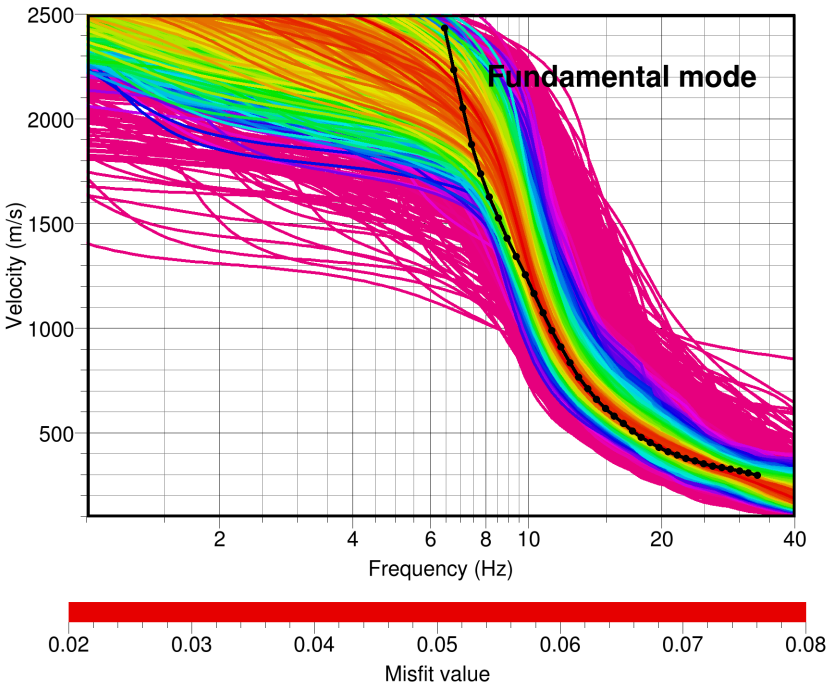

B)

Figure 17 - *Example of fitting the surface dispersion data within the global optimization procedure. Different colors represent different misfit between the observed (in black) and the modeled dispersion curves during the search (A, Rayleigh; B, Love).*

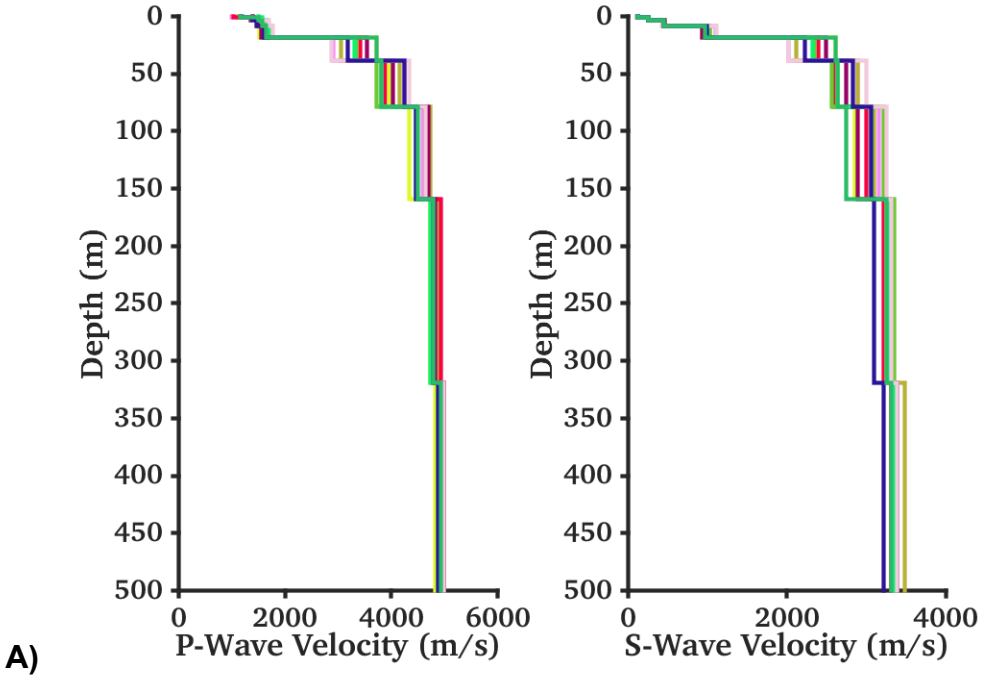

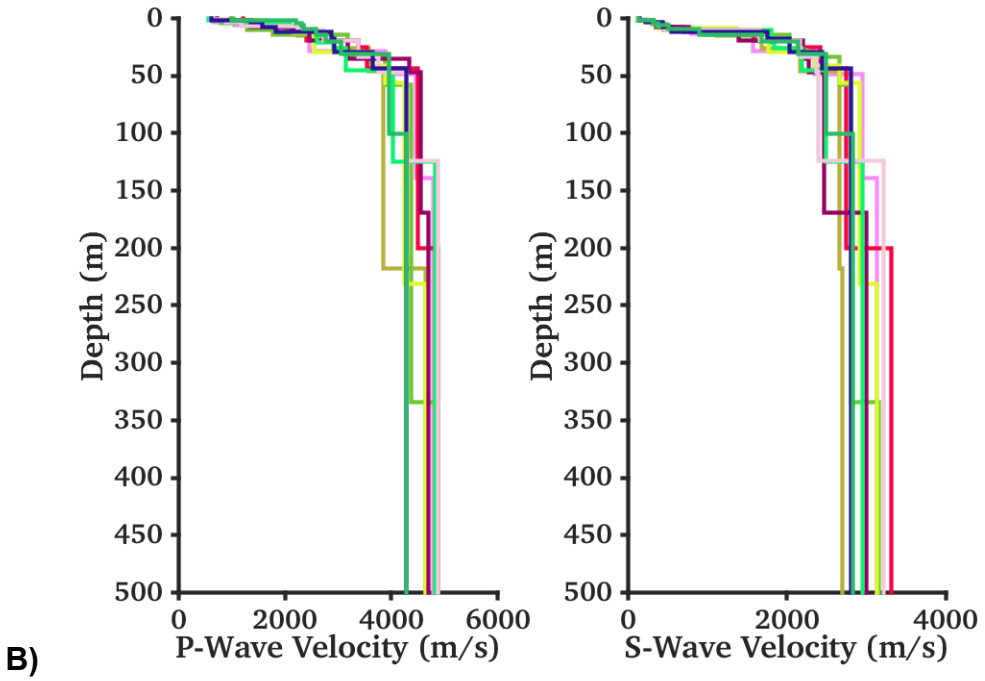

Figure 18 - *Collecting the best fitting models from the ten separated inversion runs using the free-layers (A, top) and fixed-layers (B, bottom) parameterization schemes.*

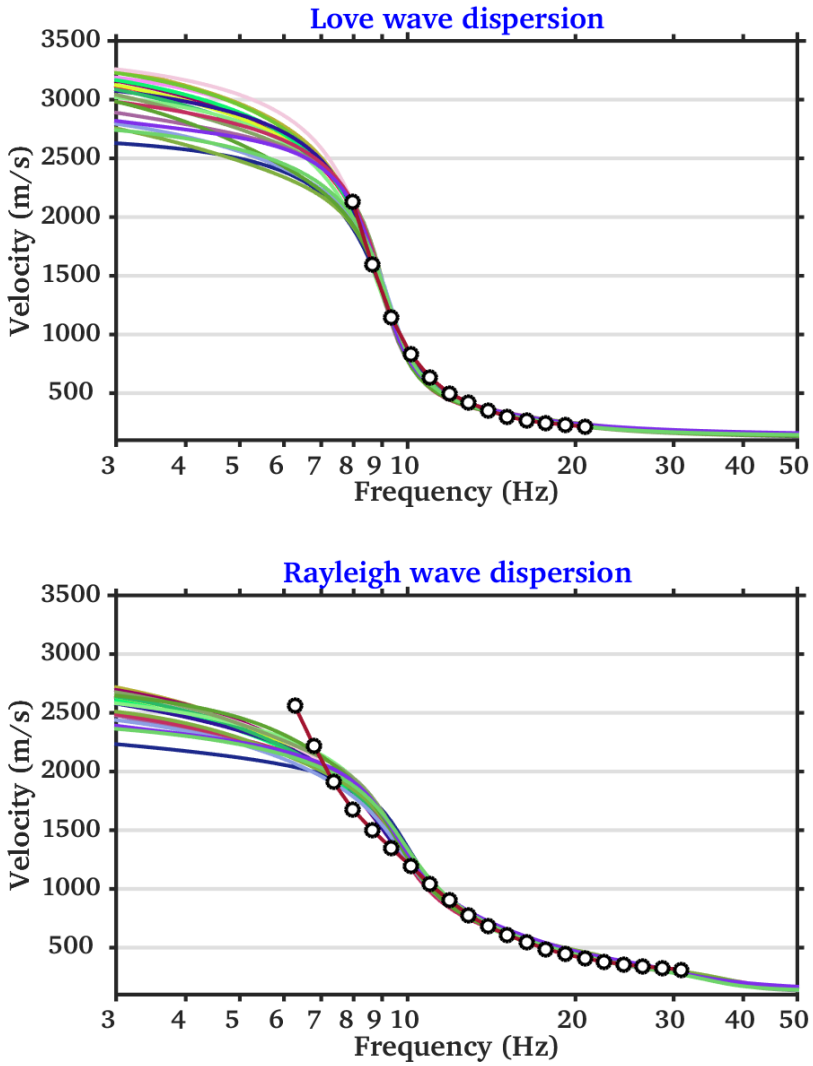

Figure 19 – *Rayleigh and Love dispersion curves computed from the 20 best fitting models of the two proposed interpretation schemes (free and fix layers).*

To parameterize the velocity model, two different approaches were implemented. The first one consisted in setting up an eight-layer model with fix interface depths. In such a case the free inversion parameters are then the velocities (P and S) and layer thicknesses. In the second case, a free-thickness layer approach was used. The advantage of the former method stays in the possibility to better resolve sharp velocity interfaces, while the second is less unique and better constraints the seismic velocity. The two approaches have to be nevertheless considered complementary, and they should provide consistent results.

Ten inversion tests (*runs*) were performed for each of the two model schemes, in order to minimize the effect related to a possible unfavorable initial randomization of the parameter space. The best fitting model from of each run was then collected (**Figure 18** and **Figure 21**) and used later on for the computation of the derived soil parameters.

In more detail, the inverted velocity models (Vs and Vp) are gradient-like, with a faster increase in velocity in the first 50m, followed by a more regular part of nearly constant velocity. This might be expected from the local geological information. The retrieved profile is well explained by both Love and Rayleigh dispersion curves (**Figure 19**) - which show a visible kink at about 10Hz - and by the high frequency part of the H/V spectral ratios (f_0 and right flank of the maximum), considered representative of the Rayleigh wave ellipticity function (**Figure 20**). Theoretical ellipticity doesn't nevertheless match the whole H/V function, likely due to the presence of additional wave contribution (e.g. SH waves) in the ambient vibration wave-field.

By considering the minimum available frequency of the surface-wave analysis, and by analyzing the scattering of the inverted models (**Figure 21**), it is realistic to assume the velocity profiles to be reliable down to a depth of about ~200m. Below this value no direct constrain is available from data, and the velocity values are obtained by pure extrapolation.

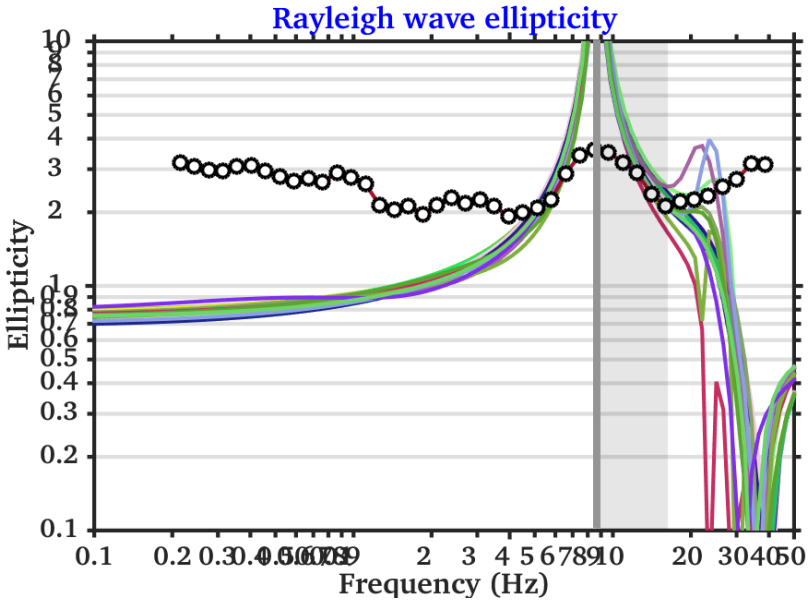

Figure 20 - *Rayleigh wave ellipticity curves computed from the best fitting models of the two proposed interpretation schemes (free and fixed layers), compared with average H/V spectral ratio from configuration R1 (scaled by sqrt(2)). Only the high frequency maximum (f_0) and the related right flank were used during the inversion.*

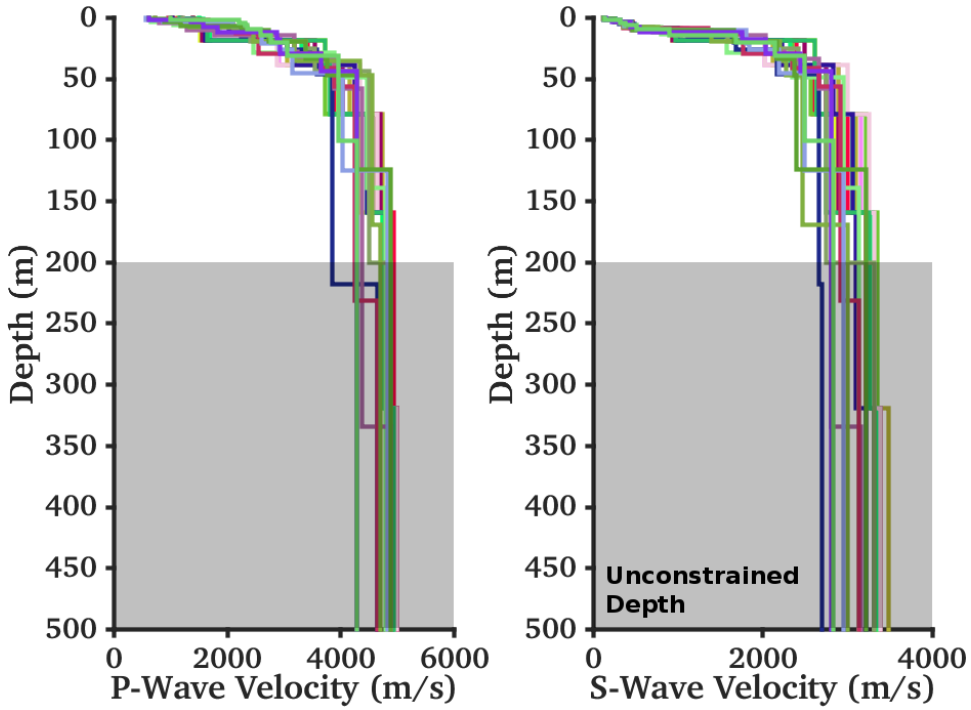

Figure 21 - *Comparison of all the best models from the two parameterization schemes (free and fixed layers). The two approaches produce consistent results. The depth of about 200m is considered approximately the maximum resolved depth.*

11. Engineering soil parameters

The ensemble of all the best inverted velocity profiles is then used to derive average soil parameters like the VsZ (average travel-time S-wave velocity over the depth Z, including Vs30, Table 1) and the quarter-wavelength (QWL) average velocities (Joyner et al., 1984) for a range of frequencies between 0.6 and 30Hz (**Figure 22**). The former is a standard parameter for the classification of ground-types in most building codes and in ground motion prediction equations. The latter is a parameter useful for the empirical estimation of the site-response and to assess the sensitivity of the seismic wave-field to the different depths. It has to be noticed that these two parameters are derived separately from all the best S-wave velocity models obtained from the inversion, and the results is finally averaged to improve statistics.

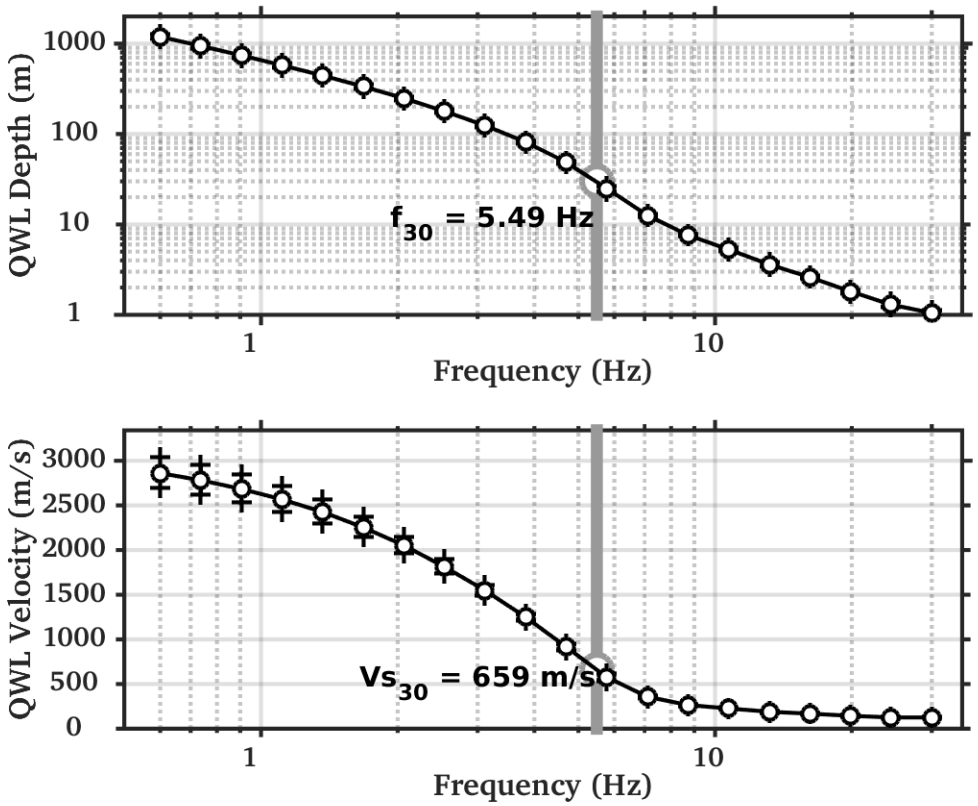

Figure 22 - *Quarter-wavelength representation of the inverted S-wave velocity profiles. Top: the depth-frequency dependency. Bottom: the QWL average velocity. The Vs30 value is indicated with its corresponding QWL frequency.*

12. Amplification models

Site amplification functions have been computed using two different approaches: the S-wave transfer function for vertical propagation and the quarter-wavelength amplification. In general the first method is used to evaluate the resonance characteristics of the site, while the second is more useful to assess the effect of the velocity contrasts between the lowermost rock layer (as reference) and the different QWL averaging depths. The two amplification functions are then corrected for the Swiss rock reference velocity profile as defined in Poggi et al. (2011), according to the procedure described in Edwards et al. (2013). Given the lower velocities in the uppermost part of the EMING profile compared to the Swiss reference, the final corrected amplification function shows a lower average amplification level at high frequencies than the uncorrected (**Figure 23**), while low frequency part is nearly asymptotic.

Averaging depth (m)	Vs-mean (m/s)	St.Dev.
5	220.99	5.10
10	306.21	4.43
15	402.68	5.70
20	489.82	12.72
25	578.41	11.79
30	**659.08**	**11.68**
40	803.27	13.97
50	932.00	13.75
75	1191.70	16.88
100	1392.32	24.76
150	1683.37	40.38
200	1895.09	52.10

Table 1 - *Average travel-time velocities at different depths. Vs30 is highlighted.*

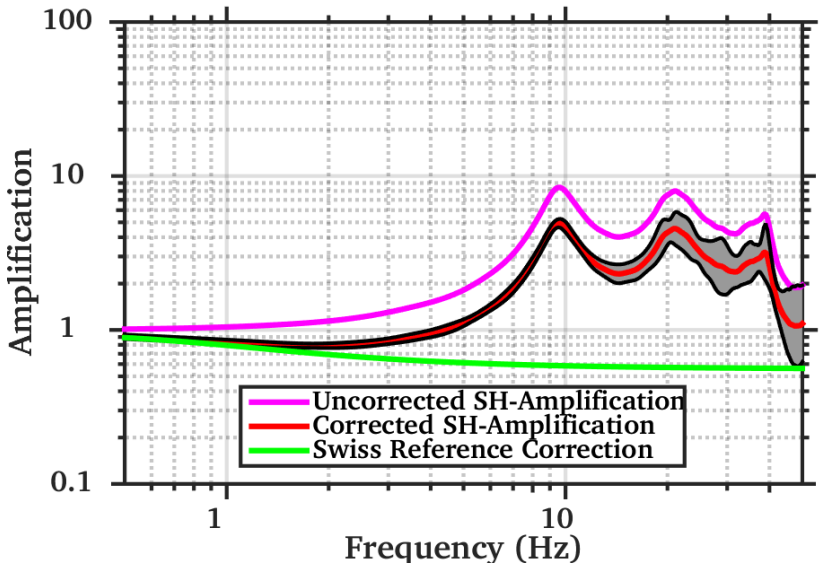

Figure 23 - *Correcting the SH-wave transfer function for the Swiss (rock) reference conditions (Poggi et al. 2011). The final corrected amplification function shows a lower (average) amplification at high frequencies than the uncorrected.*

Amplification functions using the transfer function and the quarter-wavelength approach are comparable (**Figure 24**), even if the transfer function provides a slightly larger amplification, because of the presence of some weak resonance peaks. At low frequencies both methods converge to the same amplification level. It has to be notice that the amplification functions do not include attenuation at this stage of the analysis, as the quality factors of the site are too uncertain.

A good matching is obtained by comparison between the one-dimensional transfer function and the empirical amplification from spectral modeling of low-magnitude earthquakes as described in Edwards et al., 2013 (**Figure 25**). This confirms the reliability of the inverted velocity profile in light of the current assumptions of one-dimensionality.

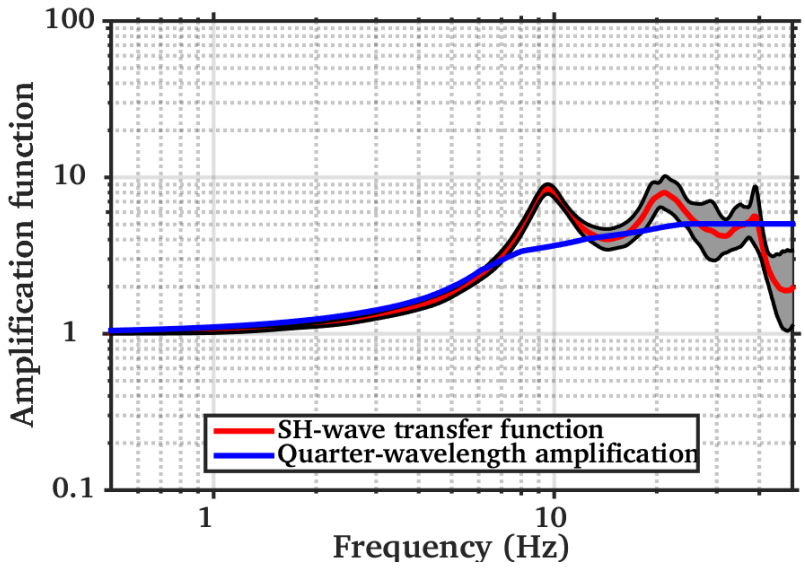

Figure 24 - *Comparison of amplification functions computed using the SH-wave transfer function and the quarter-wavelength formalism on the inverted velocity models.*

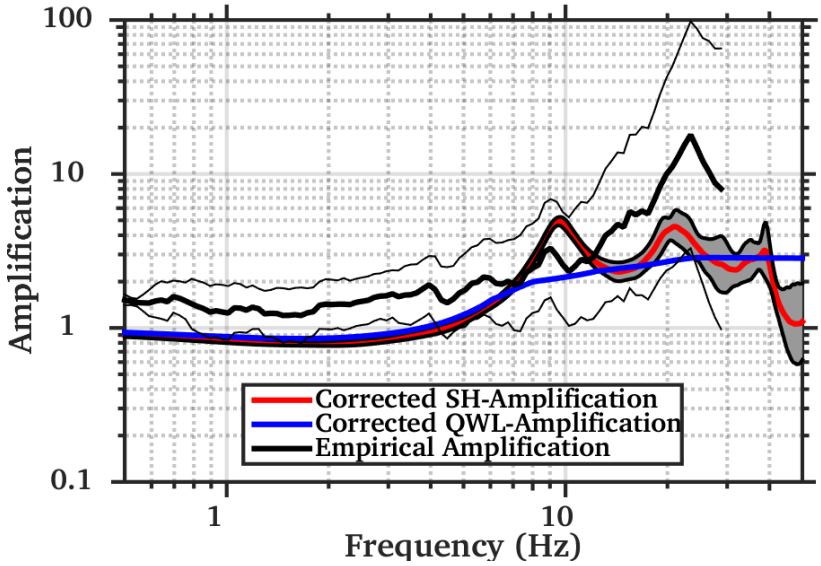

Figure 25 - *Comparison of amplification functions computed using the SH-wave transfer function and the quarter-wavelength approach with empirical observation from spectral modeling of low-magnitude earthquakes. All functions are referenced to the Swiss rock reference model (Poggi et al. 2011).*

REFERENCES

Capon, J., 1969. High resolution frequency wavenumber spectrum analysis, Proc. IEEE, 57, 1408-1418.

Burjanek, J., G. Stamm, V. Poggi, J.R. Moore, and D. Fäh [2010], "Ambient vibration analysis of an unstable mountain slope", Geophys. J. Int., Vol. 180, pp. 820-828.

Edwards, B., C. Michel, V. Poggi and D. Fäh (2013). Determination of Site Amplification from Regional Seismicity: Application to the Swiss National Seismic Networks. Accepted for publication in Seismological Research Letters.

Joyner, W. B., R. E. Warrick and T. E. Fumal (1981). The Effect of Quaternary Alluvium on Strong Ground Motion in the Coyote Lake, California, Earthquake of 1979, Bulletin of the Seismological Society of America, 71, 1333-1349.

Poggi, V., B. Edwards and D. Fäh (2011). Derivation of a Reference Shear-Wave Velocity Model from Empirical Site Amplification, Bulletin of the Seismological Society of America, 101, 258-274.

Poggi, V. and Fäh D., 2010. Estimating Rayleigh wave particle motion from three-component array analysis of ambient vibrations. Geophys. J. Int., 180-1, 251-267.